Journal of Controlled Release 167 (2013) 290–300

Contents lists available at SciVerse ScienceDirect

Journal of Controlled Release

journal homepage: www.elsevier.com/locate/jconrel

Stratum corneum permeabilization with photoacoustic waves generated by piezophotonic materials

Gonçalo F.F. Sá [a], Carlos Serpa [a,b], Luis G. Arnaut [b,*]

[a] LaserLeap Technologies, IPN, R. Pedro Nunes, 3030-199 Coimbra, Portugal
[b] Chemistry Department, University of Coimbra, 3004-535 Coimbra, Portugal

ARTICLE INFO

Article history:
Received 28 January 2013
Accepted 10 February 2013
Available online 16 February 2013

Keywords:
Photoacoustic waves
Dermal drug delivery
Piezophotonic materials

ABSTRACT

Photoacoustic (PA) waves generated by short laser pulses absorbed by piezophotonic materials are shown to permeabilize the stratum corneum to large molecules and proteins. Two minutes of such PA waves at a laser pulse frequency of 20 Hz increase the transepidermal water loss (TEWL) of healthy human skin by a factor of 2.5, and the skin relaxes to normal two minutes later. The intraepidermal delivery of Green Fluorescence Protein (GFP) in minipigs with this method does not lead to observable adverse effects. The distinctive features of the piezophotonic materials are the high light-to-pressure conversion efficiency and the generation of PA waves with the duration of the laser pulses. Such features combine to yield broadband pressure waves with steep pressure gradients that are capable of permeabilizing the stratum corneum.

1. Introduction

The remarkable protection against chemicals and pathogens provided by the skin also limits transdermal delivery to a very small set of the medicines available today [1]. The physicochemical properties of good skin penetrants are even more restrictive [2] than those of drugs intended for oral delivery [3]. The permeability of the skin can be increased with topical formulations, or transdermal patches, containing chemical penetration enhancers, but there are fundamental constraints in their design associated with their skin irritation potential [4]. These difficulties motivated the development of a wide range of physical methods to actively deliver drugs through the skin. The use of electrical (iontophoresis, electroporation), mechanical (microneedles, ballistic injectors), thermal (thermal ablation) or pressure (ultrasound, stress transients) methods opened new perspectives for the transdermal delivery of drugs [5–9]. However, the need for safe, painless, efficient and affordable transdermal delivery of drugs remains unfulfilled and the most relevant alternative to the oral delivery of drugs is still the use of hypodermic needles, regardless of pain, contaminations and waste. This work presents a physical method based on ultrahigh-frequency ultrasound waves with steep pressure gradients that transiently perturb the outer-skin barrier and facilitate drug delivery.

The grand challenge of transdermal drug delivery is not just to bypass the efficient protection of our skin against the ingression of chemicals and pathogens. Transdermal delivery aims at painless and fast transport of drugs through the skin without damaging it, such that the skin recovers its protective function and original appearance shortly after the treatment. The main contributor to the impermeability of the skin is its outermost layer, called stratum corneum (SC), although it is only 10 to 20 μm thick. It is made by a dozen layers of hardly packed nonliving corneocyte cells embedded in a mixture of lipids with high spatial organization [10]. Most molecules penetrate the skin by diffusion through the intercellular lipids, a narrow and tortuous path around the corneocytes that is highly constrained by structural and solubility requirements. Molecules heavier than 400–500 Da are unable to find sufficiently wide defects in the intercellular lipid matrix to start diffusing through the lipidic parts of the SC barrier and remain essentially confined to the skin surface [6]. Hydrophilic transepidermal pathways can be found between corneocyte clusters but impose even more strict size restrictions [6].

The steady-state water vapor flux crossing the skin to the external environment, or transepidermal water loss (TEWL), reflects the barrier function of the skin. The value of TEWL changes with the anatomical site, environmental conditions and, to some extent, with the equipment employed in the measurement [11–15]. TEWL measurements often employ the ventral forearms of healthy volunteers, and values between 5 and 14 g/(m^2 h) were reported. This should not be interpreted as lack of precision of the measurements, but rather as warning against comparison between absolute measurements performed in different laboratories. The precision of the measurements in a given setting is usually high, e.g. 6.4 g/(m^2 h) with a standard deviation of 2.08 g/(m^2 h) [11] or 14.5 ± 3.2 g/(m^2 h) [13], provided that the same equipment is used with the same protocol and under the same environmental conditions. Although the correlation between the TEWL and the percutaneous absorption rates of drugs may not be entirely general, it is nevertheless widely recognized that the TEWL is a measure of the skin barrier function and permeability [14,16–19].

* Corresponding author. Tel.: +351 239 854484; fax: +351 239 827703.
E-mail address: lgarnaut@ci.uc.pt (L.G. Arnaut).

0168-3659
http://dx.doi.org/10.1016/j.jconrel.2013.02.005

The path through the intercellular lipids can be facilitated expanding the extracellular domains of the SC, and enhanced transdermal delivery of large drugs was observed when high-frequency (16 MHz) ultrasound [20], low-frequency (20–25 kHz) sonophoresis [21,22] or just the use of surfactants [23] expanded lacunar domains. Shock waves are also believed to use this mechanism to increase the permeability of the skin [24,25]. This work shows how to permeabilize the stratum corneum using photoacoustic (PA) waves generated by the thermoelastic expansion of materials characterized by efficient and ultrafast conversion of light into pressure at optical power densities (or fluence rates) of portable pulsed lasers (I_L<10 MW/cm^2 per pulse, e.g. a 100 mJ/cm^2 laser pulse with a duration τ_L=10 ns). Experiments first performed with minipigs, in view of the similarity between their skin and human skin, and then with healthy volunteers, show that the SC becomes very permeable to large molecules and proteins for a few minutes after the application of PA waves and then totally recovers its protective function. The PA waves employed in this work do not have the high intensities and low frequencies required to produce cavitation. On the other hand, they have very sort durations, as short as the nanosecond laser pulses employed to generate them, and even with moderate pressure amplitudes, they achieve very accentuated pressure gradients. We show that the PA waves generated with our method produce a pressure gradient of more than one bar across a single cell, as illustrated in Fig. 1, and this is the origin of the perturbation of the SC structure.

2. Theory

Thermoelastic expansion is usually considered an inefficient method to convert a pulse of light into a pressure wave because the observed optical-to-acoustic energy conversion efficiencies are typically $\eta_{PA}<10^{-5}$ [26–28]. However, this is much lower the theoretical efficiency of photoacoustic conversion. The maximum pressure amplitude generated by thermoelastic expansion after absorption of a laser pulse with the optical power density I_L is given by [29]

$$p_{max} = I_L \gamma / c_s \quad (1)$$

where the Grüneisen coefficient γ characterizes the thermoelastic behavior of materials and c_s is the longitudinal speed of sound. Considering that for $p<<\rho c_s^2$, where ρ is the density, the average sound power density (i.e., the rate of energy flow through a unit area perpendicular to the direction of propagation) is [30]

$$I_s = p^2/(\rho c_s) \quad (2)$$

and we anticipate that the efficiency of light-to-pressure transduction increases with the optical power density

$$\eta_{PA} = I_s/I_L = I_L \gamma^2 / \left(\rho c_s^3\right) \quad (3)$$

This relation holds true below the ablation threshold of the material. For polystyrene (γ =0.70 [31], c_s=2400 m/s and ρ=1050 kg/m^3 [32]) doped with a dye absorbing all the incident light, the maximum PA conversion efficiency is limited by its ablation threshold at I_L= 15 MW/cm^2 [33], and is η_{PA}=0.005. Higher conversion efficiencies can be expected for materials with high Grüneisen coefficients and higher ablation thresholds.

These theoretical estimates reveal that PA conversion is not intrinsically inefficient. The conversion efficiency can be experimentally improved with laser pulse shaping and materials that meet the following properties:

(i) Thermal confinement – the laser pulse duration is shorter than the thermal diffusion time, $\tau_L<\tau_d$, where $\tau_d=(\rho\ C_p)/(\kappa_t\ \mu_a^2)$. Under this condition, the short duration of the laser pulse restricts the energy deposition to the absorbing volume [34].

(ii) Optical confinement – the strong light absorption by the material makes the acoustic relaxation time τ_s shorter than the laser pulse, $\tau_s<\tau_L$, where $\tau_s=1/(\mu_a c_s)$. Under this condition, the spectral band of the laser pulse will determine the spectral band of the PA wave [35], and short laser pulses give ultrahigh frequency waves.

In the expressions above, C_p is the specific heat capacity, μ_a the linear absorption coefficient and κ_t the thermal conductivity of the absorbing material. It is implicit in the optical confinement limit that the electronic states formed by the absorption of light decay back to their ground state in a time shorter than the duration of the laser pulse, as in the compounds used as references for photoacoustic

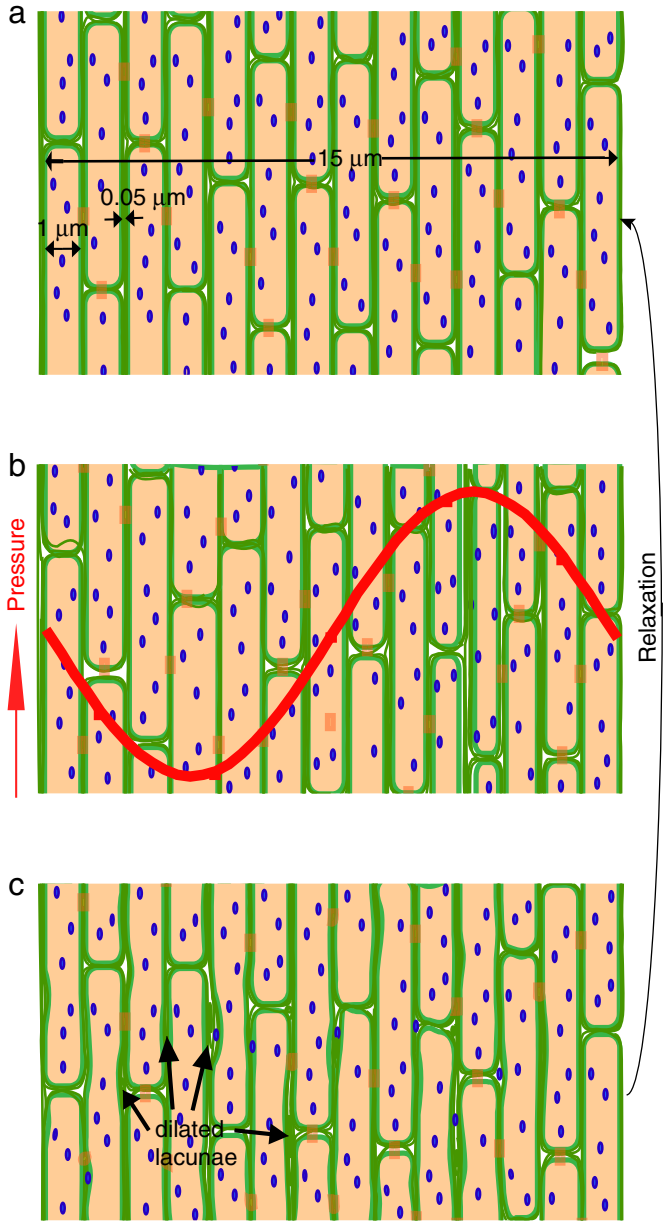

Fig. 1. Rationalization of the increased skin permeability following the application of photoacoustic waves with frequencies above 100 MHz. a, Unperturbed stratum corneum, shown as 14 layers of tightly packed corneocytes with hydrophilic domains (blue) separated by intercellular lipid lamellae (green), where the diameter of the corneocytes (40 µm) is not represented to the scale. b, Compressive front and rarefaction tail of a photoacoustic wave with a steep pressure gradient traversing the stratum corneum and producing very fast pressure changes. c, Perturbed stratum corneum with expansion of the lacunar spaces where the organization of the lipid matrix is changed and takes some time to relax to the original structure, which facilitates the diffusion of drugs through the expanded spaces, which correspond to pores in a 3D view.

calorimetry [36,37]. We refer to $\tau_s<\tau_L<\tau_d$ as the limits of photoacoustic spectral confinement.

The efficiency of PA conversion can also be increased with appropriate design of the conversion device. First, the generation of pressure waves by thermoelastic expansion increases when the absorbing medium is confined by rigid boundaries [38,39]. Second, the peak pressures obtained by thermoelastic expansion scale with the reciprocal of the thickness (h) of absorbing material for the same amount of energy absorbed [40],

$$\Delta p = \Delta H_{th}\gamma/h \quad (4)$$

where ΔH_{th} is the thermal energy released per unit area, because the thermal energy is released in a smaller volume. However, a word of caution is in order. The limits of photoacoustic spectral confinement require, for example, that an 8 ns laser pulse is "totally" absorbed by a material with $\mu_a > 1100\ cm^{-1}$ at the laser wavelength, which may be difficult to fabricate.

Biagi et al. reported heavily absorbing films designed to maximize the value of η_{PA} and obtained a conversion efficiency $\eta_{PA}\approx 10^{-6}$ [27]. This disappointing efficiency can be assigned to the low power densities employed: $I_L = 0.4\ MW/cm^2$ produced a PA wave with $p_{max} = 0.1$ bar. Guo et al. developed photonic crystal-metallic structures with a layer of an elastomer and operated in a total-internal-reflection geometry to obtain $p_{max} = 2.4$ bar with $I_L = 1.8\ MW/cm^2$ [41], i.e. $\eta_{PA}\approx 3\times 10^{-6}$. This is one of the highest conversion efficiencies reported in the literature, although it did not make use of confinement by rigid interfaces. We designed light-to-pressure transducer materials guided by the relations described above. These materials are very thin (thickness<100 μm) and strongly absorbing ($\mu_a > 100\ cm^{-1}$) films that are incorporating dyes with ultrafast radiationless decays (transient lifetimes <1 ns). We name such materials "piezophotonic". A polystyrene-based piezophotonic material with $\mu_a = 500\ cm^{-1}$ is in the limit of generating a PA wave with the time dependence of a laser pulse with $\tau_L = 8$ ns.

3. Materials and methods

3.1. Piezophotonic materials and pressure measurements

Light-to-pressure transducer films were casted from a mixture of polystyrene and either Mn^{III} 5,10,15,20-tetraphenylporphyrinate (Mn-TPP) or Mn^{III} 5,10,15,20-tetraundecylporphyrinate (Mn-TUP) using an Elcometer 3505 cube film applicator. Polystyrene and toluene were mixed and stirred until the entire polymer was dissolved. The dye was then added to polystyrene/toluene and all the mixture was stirred until the dye was completely dissolved. Air bubbles resulting from stirring were eliminated placing the polystyrene/toluene/dye in an ultrasonic bath for some minutes. Finally, the mixture was poured into the mold and spread on a clean glass sheet. The films deposited by casting were dried at room temperature and then removed from the glass sheet. The thicknesses of the films were measured with a digital micrometer.

Nanoporous titania films were prepared from a TiO_2 sol (HT/SP from Solaronix). The colloidal thin films, [1.75; 2.5; 3.25] μm, were distributed in a screen-printing device previously acquired with required thicknesses. The larger films [5; 7.5] μm were applied using the squeegee print method. The colloid was distributed with a glass rod sliding over a rim circle made with Scotch Magic adhesive tape (3M). After air drying, the films were sintered in an oven at 500 °C for about 90 min. Mn^{III} 5,10,15,20-tetrakis(4-sulphonylphenyl)porphyrinate acetate (Mn-TPPS) was adsorbed to the surface of nanostructured titania by immersing glass slides coated with TiO_2 in an ethanol solution of the dye for the period of time required to attain the desired absorptivity. The absorbances at 471.5 nm were matched at 0.5. These methods produce a uniform titania layer with a homogenous monolayer of dye adsorbed onto it [42].

The thermoelastic expansion that gives rise to PA waves is, in principle, non-destructive. In practice, signs of material fatigue are apparent after ca. 30,000 laser shots. This is visually characterized by a change in color and a decrease in opacity of the films. The films used in the experiments described below were regularly replaced.

3.2. Topical formulations

The permeability of the skin of minipigs was tested with a bacteriochlorin (molecular weight 1.1 kDa) of interest as a photosensitizer in the photodynamic therapy (PDT) of cancer [43,44], and with Green Fluorescent Protein. The bacteriochlorin was a gift from Luzitin SA (Portugal), and Green Fluorescence Protein (GFP) was obtained from Merck Millipore. The bacteriochlorin and GFP were incorporated in topical formulations, as described below, and applied to the skin of minipigs. Bacteriochlorins are particularly suitable for these assays because, in addition to the molecular weight of 1.1 kDa, they are stable and have a very characteristic fluorescence with a peak near 750 nm. GFP has a molecular weight of 28 kDa and is also very convenient to illustrate the increased permeability of skin with the application of PA waves because its characteristic fluorescence at 510–550 nm is simple to follow.

The bacteriochlorin uptake into the skin was tested using a Carbopol type gel with high water percentage. The gel preparation was done in three steps. First, the solvents of the gel base were introduced in the following order and stirred magnetically at 2400 rpm: 6% of glycerin, 1.35% of triethanolamine, 1% of carbopol 940, 15% of ethanol absolute and 76.65% of distilled water. Next, the bacteriochlorin was dissolved in the solvent mixture ethanol:propylene glycol:oleic acid (16.6:36:2, % w/w), subject to 1 min of ultrasound to assure complete solubilization, and added to the gel base in order to make 44.9% of the formulation. The final concentration of the bacteriochlorin in this gel was 0.5%. A formulation with 5% of bacteriochlorin, compensated with the reduction in gel base, was also tested and did not give significantly different results. A formulation with Azone (4%) in lieu of oleic acid, and compensated by a reduction of ethanol, was prepared with 1% of bacteriochlorin and tested under similar conditions. To avoid degradation and maximize polymer swelling, the gels were prepared 24 h before the experiment and kept at +4 °C.

GFP was dissolved in the amount of water employed to make the gel base and then the other components of the gel base were added, together with Azone (4%). The final concentration of the GPF in the gel base was 0.1%, and this was the topical GFP formulation employed in this work.

The rational to include a permeation enhancer in the topical formulation was to improve the passive delivery of the bacteriochlorin and GFP. This allows us to compare the best passive delivery with the dermal delivery with PA waves. The detailed studies on the optimization of the formulation for passive delivery will be published elsewhere because they are not relevant for the comparison between active and passive delivery. The Supplementary Data also presents results obtained with Azone in the place of oleic acid and also with the porphyrin precursor of the bacteriochlorin mentioned above.

3.3. Generation of photoacoustic (PA) waves

The experiments with excitation at 484 nm and 471.5 nm employed an EKSPLA OPO model PG-122 pumped by an EKSPLA NL301G Nd:YAG laser delivering 4–6 ns pulses. Exploratory work with minipigs and the delivery of GFP employed a Spectra Physics Quanta Ray 130 Nd:YAG laser to generate PA waves. The delivery of the bacteriochlorin and the work with volunteers used a portable Quantel Big Sky Ultra 50 Nd:YAG including a second harmonic generator (532 nm wavelength output, 8 ns pulse duration) to generate the PA waves. In particular, the TEWL experiments employed a Quantel laser with pulse energy densities of 50 mJ/cm^2. The laser

pulse was directed to an optical fiber that delivered the light to the light-to-pressure transducer. This material was confined between an optical window and a mirror using silicone as acoustic coupler. The mirror reflected the light back into the piezophotonic material and protected the skin from the laser light. The photoacoustic waves were transmitted to the skin by physical contact between the back of the mirror and the skin and the acoustic coupling was improved placing a thin layer of silicone between the back of the mirror and the skin of the volunteers, or a thin layer of the topical formulation between the back of the mirror and the minipig skin.

Pressure wave measurements were made with a calibrated needle hydrophone model MH28 from Force Technologies or with Panametrics (Olympus) contact piezoelectric transducers (100 MHz and 225 MHz), connected to a DPO7254 Tektronix digital oscilloscope.

3.4. Transdermal delivery in minipigs

In vivo tests employed minipigs obtained from IMIDRA (Instituto Madrileño de Investigación y Desarrollo Rural, Agrario y Alimentario) - Aranjuez (Madrid). They were aged 6–8 months, white with brown spots, and with weights ca. 60 kg. They were received at INRB, Vale de Santarém (Portugal), where they were accommodated in individual boxes with 1.5 m^2, feed with a standard diet for pigs and water *ad libidum*, for an acclimation period of three weeks. The study was performed in accordance to the Portuguese ethical guidelines on a license granted by *Direcção de Serviços de Saúde e Protecção Animal*, ref. 0420/000/000/2007, with the assistance of veterinary surgeons. Access to food was suspended 24 h before treatment. The backs of the animals were shaved 24 h prior to the *in vivo* application of the dermatological formulations. The formulations, laser system and piezophotonic materials employed in these experiments were described above. All procedures were carried out under anesthesia. The pre-medication given 30 min in advance was: Azaperone (Stresnil® – Veterinaria ESTEVE – Spain), 2 mg/kg intramuscular injection + atropine sulfate, 50 mg SC. The induction was done with ketamine (Clorketam® – Vétoquinol, France), 20 mg/kg, intramuscular injection. The anesthesia was maintained with endotracheal intubation, using spontaneous ventilation with 2–3 L/min of oxygen + 3% isoflurane (Isoflo® – Veterinária ESTEVE, Spain). The skin biopsies were collected under the anesthesia described above. After the collection of the biopsies, the animals were killed with an overdose of sodium thiopental (25 mg/kg) + 20 ml of 7.5% potassium chloride.

In vivo transdermal delivery and skin biopsies were made with the following procedure in a temperature-controlled room in the presence of the investigators and two veterinary surgeons: a) The back of the minipig was cleaned with ethanol soaked in medical cotton and allowed to dry. b) Square areas with 1 cm size was delimitated on the back of the minipig using adhesive tape, resulting in 15 different squares in each animal. c) The contact times were planned (i.e., 15 min, 30 min, 1 h, 2 h, 3 h) and marked on the adhesive tape. d) Starting with the longest contact time, the formulation containing bacteriochlorin or GFP, described above, was applied in the designated area with a spatula, leaving a uniform 1 mm layer of the formulation. e) The device to generate PA waves, described above, was gently pressed against the formulation and the laser was fired. f) The device was removed and more formulation was added to reform the 1 mm layer of formulation. g) The formulation was occluded with Tegaderm® and aluminum foil for the desired amount of time. h) After the time difference between the longest and second-to-longest contact times elapsed, the skin area assigned to the second longest contact time was treated same way. i) The appropriate timings were followed in the application of the formulation to each one of the skin areas in such a way that all the contact times terminated for all the skin areas at the same time. j) At the simultaneous end of all the planned contact times, Tegaderm® and aluminum were rapidly removed from all skin areas and the formulation was thoroughly cleaned with absorbing paper and then with ethanol soaked in medical cotton. k) Two skin biopsies were then rapidly collected from each area. l) Immediately after excision the biopsies were frozen until further use. m) The minipig was sacrificed as described above. One set of the biopsy punches was used for extraction and quantification of the amount of the bacteriochlorin in the skin, whereas the other set was analyzed using fluorescence microscopy for the depth of penetration. Passive delivery studies followed the same procedure, with the same formulations, except that the PA waves were not applied.

3.5. Analytical methods

The extraction and quantification of the bacteriochlorin in one of the sets of biopsies were performed according to the following steps: a) The skin biopsy was sectioned in the smallest pieces possible with a scalpel. b) These pieces were transferred to a cup glass with 2 ml of dichloromethane and crushed with a shredder, YSTRAL Micro Shaft 6G. c) 8 ml of dichloromethane were added to the resulting mass and allowed to stand for 6 h. d) A volume of 3 ml of the supernatant was transferred to a quartz cuvette and its fluorescence intensity was recorded. The amount of the bacteriochlorin present in each skin biopsy was determined using a calibration curve made with solutions having a known concentration of the bacteriochlorin in dichloromethane. The steady-state fluorescence of the bacteriochlorin was measured with a Horiba-Jovin-Yvon Spex Fluorog 3-2.2 spectrophotometer in a 1 cm quartz cuvette and corrected for detector wavelength dependence.

The measurement of the depth of penetration of the bacteriochlorin or GFP in the other sets of biopsies followed the steps: a) Tissue fixation was made immersing the tissue in paraformaldehyde (4% in aqueous solution) for at least 24 h, and then in a 25% sucrose solution for at least 48 h; alternatively, some samples were directly frozen in dry ice. b) The tissue was frozen in dry ice and then mounted on a holder with Tissue-Tek O.C.T. Compound (Sakura Finetek Europe B.V., Zoeterwoude, Netherlands). c) The tissue was cut in slices with controlled thicknesses selected between 25 and 100 μm in a cryostat. d) The skin slices were collected in microscope slides and kept refrigerated for microscopy. Fluorescence microscopy was measured with an Olympus BX51M fluorescence microscope equipped with a UV mercury lamp (100 W Ushio Olympus), using a resolution of 1/4.5 and amplification of 10×. The 515 nm excitation cube and the 600–800 nm emission cube were used for the bacteriochlorin. The 470–495 nm excitation cube and the 510–550 nm emission were employed to obtain the GFP fluorescence. The images were processed in a personal computer by an Olympus Digital DP70 video camera, and analyzed with Olympus DP Controller 2.1.1.176 and DP Manager 2.1.1.158 software. Confocal fluorescence of the bacteriochlorin was performed with a LSM 510 Meta (Carl Zeiss, Jena, Germany) confocal microscope, with a ×63 oil immersion objective (Plan-Apochromat, 1.4 NA; Carl Zeiss), using $\lambda_{ex} = 514$ nm, $\lambda_{em} \geq 650$ nm, laser power at 5% and an amplification 40×. Confocal fluorescence of GFP in skin slices from experiments with *post mortem* minipig skin was visualized under a Leica TCS Sp5 confocal microscope using 488 nm excitation and 510–550 nm emission light. The microscopy is inverted (DMI6000) with a water apochromatic objective of 63′ and numeric aperture of 1.2. Before connecting the confocal mode, the samples are observed with a sodium lamp, as the radiation source, and with Rhod-DOPE as a fluorescent filter. The 3D projections were obtained using the analysis software of Leica®. The sample was excited with the 495 nm line of laser and emission recovered at 510 nm with a pinhole of 111.44 μm, using a detector voltage of 1150 V and a zoom of 1 or 3. All observations were done at 22 °C.

3.6. Transepidermal water loss (TEWL)

Healthy volunteers gave their informed consent to participate in the measurement of TEWL in both of their forearms, before and after the application of PA waves. They were informed that the application of the laser-generated PA waves was to take 2 min, and that

they could ask to interrupt the experiment at any time. Subjects with a history of atopic dermatitis, asthma, contact dermatitis or allergy were excluded from the study. Each subject was tested in both forearms with the same procedure, except that in the first procedure the laser shutter was kept closed (laser OFF). The subjects were not informed that the first exposure was a control experiment. It was planned to exclude from the study the volunteers reporting discomfort in this first exposure (laser OFF), but this case was not observed and all the participants enrolled in the experiment completed it. The TEWL measurements were made with the following procedure in a temperature-controlled room in the presence of one volunteer and, occasionally a second one for acclimatization, and two investigators: a) A circular area with 1 cm diameter was marked in each forearm and cleaned with medical cotton. b) The erythema in this area was measured. c) One investigator measured the TEWL in this area for at least 1 min after stabilization of the measurements. d) A thin layer of silicone was spread over the selected area. e) The investigator pressed gently the device generating the ultrasound waves against the selected area for 2 min – the volunteer did not know of the existence of a laser shutter. f) The selected area was cleaned with medical cotton in ca. 15 s. g) One investigator measured the TEWL in this area for at least 1 min after stabilization of the measurements. h) The erythema in this area was measured again.

Transepidermal water loss (TEWL) was measured using a Courage + Khazaka open chamber probe model Tewameter® TM 300, and expressed in g/(cm^2 hr). Erythema was measured using a Courage + Khazaka probe model Mexameter® MX 18, and is expressed in arbitrary units.

4. Results and discussion

4.1. Properties of photoacoustic waves

Table 1 shows the properties of piezophotonic materials made with photoacoustic calorimetry references dispersed in polystyrene or adsorbed to TiO_2 nanoparticles. Film A immersed in water was irradiated with 40 mJ/cm^2 laser fluence using 8 ns pulse ($I_L = 5$ MW/cm^2) at 532 nm and the PA wave produced gave $p_{max} = 12$ bar, as measured with a 20 MHz needle hydrophone. This is 8% of the theoretical pressure predicted by Eq. (1) and corresponds to $\eta_{PA} = 10^{-5}$. To the best of our knowledge, this is the highest η_{PA} ever reported. The conversion efficiency could be easily improved increasing the laser power density, but the purpose of this work was to generate PA waves capable of increasing the permeability of the skin with safe laser and ultrasound powers. Thus, we did not attempt to improve η_{PA} and produce higher maximum pressures. On the other hand, the power spectrum of the PA waves is relevant for the skin permeability and was investigated in detail.

Table 1
Properties of representative piezophotonic materials and laser fluences used in this work.

Film	Material	Dye	Thickness μm	λ_{ex} nm	A	μ_a cm^{-1}	Laser fluence mJ/cm^2
A	Polystyrene	Mn-TPP	95	532	1.15	120	40 or 50
B	Polystyrene	Mn-TUP	38	484	1.4	370	50
				532	1.1	290	
C1–C5	TiO_2	Mn-TPPS	1.75–7.5	471.5	0.5	2860–670	32
D	Polystyrene	Mn-TPP	100	532	1.5	150	50
E	Polystyrene	Mn-TPP	60	532	1.4	230	50
F	Polystyrene	Mn-TUP	50	355	3.2	640	10
G	Polystyrene	Mn-TUP	30	355	>1	>330	50

The PA wave of Film A and its fast Fourier transform (FFT) are shown in Fig. 2A and B. The distribution of frequencies apparently peaks at 3.5 MHz but this frequency distribution is limited by the hydrophone response in the high frequency range. Excitation of Film B using laser pulses at 484 nm with 6 ns durations and detection with a 225 MHz transducer gave the PA wave of Fig. 2C and the distribution of frequencies of Fig. 2B. This film should produce PA waves with the duration of the 6 ns laser pulse, which should extend the useful bandwidth of the ultrasound generated to ca. 200 MHz [27,45]. Indeed, significant frequency components up to 200 MHz are present in the signal generated by Film B. The response of this transducer is within −6 dB (i.e., power reduction by a factor of 4) of its maximum in the frequency range between 98.6 and 335 MHz, which means that the decrease in the signal by −30 dB (power reduction by a factor of 1000) from 100 MHz to 250 MHz is unbiased by the transducer. Ultra-high frequencies are strongly attenuated in the materials where they propagate and the detected intensities are diminished even when the source is very close to the detector [46]. We placed Film B directly against the surface of the transducer to avoid differential attenuation of the ultrasonic frequencies and the observed maximum slightly below 100 MHz is the true maximum of the power spectrum. Fig. 2B also shows the frequencies obtained with the irradiation of a 634 μm thick commercial black polystyrene disk. The power at 50 MHz is only 1/10 of the peak power at 2.5 MHz generated by this commercial polystyrene and shows that this material does not meet the limits of photoacoustic spectral confinement. Fig. 4D shows that in the series of Films C1–C5 with a constant absorbance A and various thicknesses h, peak pressures increase as the thickness of the material decreases, as expected from Eq. (4).

The minimum pressure amplitude that satisfies the cavitation threshold increases with the ultrasonic frequency f_{US} [47,48]. In view of the deleterious effect of cavitation, the Mechanical Index of ultrasound, defined as $MI = p_{max}/\sqrt{(f_{US})}$, where p_{max} is expressed in MPa (1 MPa = 10 bar) and the ultrasonic center frequency f_{US} is expressed in MHz [49], should be lower than 0.5 [50]. Thus, PA waves with $p_{max} \leq 50$ bar are safe if $f_{US} > 100$ MHz, just like ultrasound waves with $p_{max} \leq 10$ bar if $f_{US} > 4$ MHz. A 2 min exposure time to 20 Hz 8 ns pulses of 40 mJ/cm^2, gives a temporal average of the total exposure to ultrasound below 1 W/cm^2, which is less than the exposure level of physiotherapy. Thus, these safe but moderately intense PA waves have rise times of tens of bar/ns and acoustical wavelengths ($\lambda_{ac} = 2c_s\tau_L$) of tens of microns. They generate steep pressure gradients that may transiently perturb the skin and facilitate transdermal drug delivery.

The data in Fig. 2 provides the grounds to explain in detail the skin permeabilization mechanism depicted in Fig. 1. The pulse duration $\tau_L = 6$ ns together with the sound velocity in soft tissues c_s = 1540 m/s give an acoustic wavelength $\lambda_{ac} = 18$ μm, which is approximately the SC thickness. At the laser fluence rates employed in our experiments, the PA waves generate a pressure gradient ca. 20 bar over a distance $\lambda_{ac}/2$, i.e., they can lead to pressure gradients of 2.2 bar/μm. The pressure gradient of therapeutic ultrasound with a peak pressure of 10 bar and a frequency of 1 MHz, which corresponds to $\lambda_{ac} = 1500$ μm, is 100 times lower.

Mitragotri and co-workers emphasized the difference in scales between the wavelength of conventional ultrasound and the SC thickness to conclude that mechanical effects do not play an important role in the permeabilization of the skin with ultrasound in the therapeutic frequency range [51]. Nevertheless, these authors also recognized that "mechanical effects could become increasingly important in the high-frequency range (frequency > 3 MHz)" [51]. Ultrasound with frequencies above 100 MHz produces mechanical stress commensurate with the size of cells. Pressure gradients of 2.2 bar/μm may displace the corneocytes from their native packing positions and open transient channels for the diffusion of drugs.

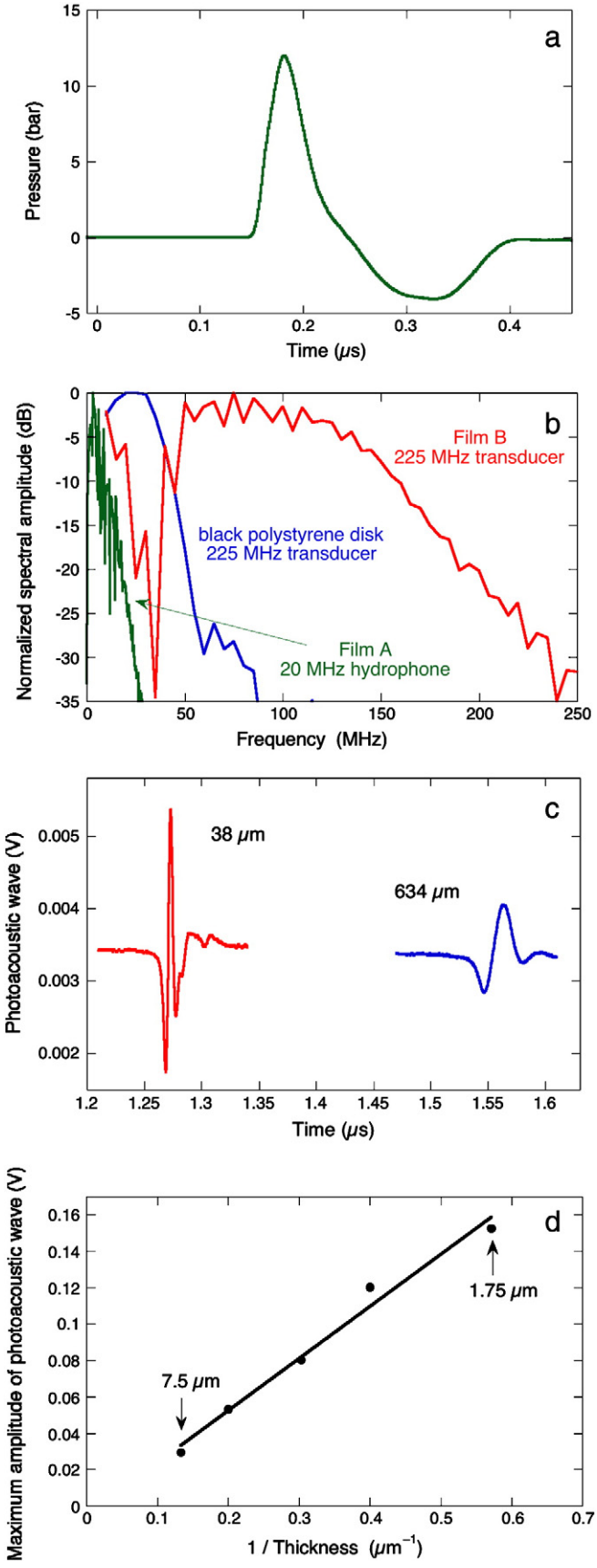

The alternative mechanism that could be considered for the effect of ultrasound in the transdermal delivery of drugs is cavitation. The steady pulsation (stable cavitation) or rapid collapse (inertial cavitation) of sub-micron gas bubbles in an ultrasound field can induce disorder in the SC lipid bilayers, thereby enhancing transdermal transport [51,52]. However, cavitation can be excluded as a possible mechanism associated with our PA waves on the following grounds:

(i) Stable cavitation is not possible in our experiments because we employ single and unfocused planar acoustic waves. We produce one PA wave with one laser pulse, and the maximum frequency of the laser pulses is 20 Hz. Thus, any bubbles eventually generated by the first PA wave have enough time to dissipate most of their energy before the second PA wave arrives.

(ii) Low-frequency sonophoresis, for which the role of cavitation is well established, employs pressure amplitudes of 2 bar and center frequencies below 0.1 MHz [53], which give MI > 0.6. On the other hand, our PA waves are characterized by $f_{US} = 100$ MHz, compressive pressure amplitudes of 10 bar and tensile stresses of 5 bar, i. e. MI = 0.05. This is well below the cavitation threshold.

(iii) High frequency sonophoresis (center frequencies between 1 and 5 MHz) is known to require much higher pressures to exceed the cavitation threshold. The measured cavitation pressure amplitude threshold was found to depend almost linearly on frequency with a slope of about 53 bar/MHz and with a 6 bar extrapolated static pressure threshold [54]. Mitragotri provided evidence for cavitation inside the SC using ultrasound at 2 W/cm^2 and $f_{US} =$ 1 MHz using long exposure times [51], but in this case the nucleation of small gaseous cavities in a negative pressure cycle of ultrasound is followed by the growth of the bubbles throughout subsequent cycles until the bubbles explode. The PA waves of our work have much higher center frequency and are not applied in resonance conditions: each PA wave is as independent event, separated by at least 50 ms from the next event.

(iv) The shock waves produced by the high-energy lasers described by Doukas [55], or by lithotripsy [56], have peak pressures between 100 and 1000 bar presented in spikes with microsecond duration. In the most favorable case, the frequency components of such waves follow the duration of the spike, which leads to $f_{US} = 1$ MHz and MI > 10. Such shock waves are most likely to produce cavitation but have the opposite properties with respect to our PA waves, which reduce the peak pressure and increase the center frequency.

4.2. Transepidermal water loss

Following the detailed characterization of the PA waves discussed above, we performed safety testing in minipigs and then evaluated how the PA could change the transepidermal water loss (TEWL) of human skin. Twenty-one healthy volunteers (18–25 years of age) from a population of medicinal chemistry students at the University of Coimbra gave their informed consent to participate in blind TEWL measurements before and after the application of PA waves in their ventral forearms for 2 min. One measurement was made in one forearm of the volunteer with the laser OFF and another one in the other forearm the

Fig. 2. Properties of photoacoustic waves. a, Pressure wave produced by Film A upon absorption of a 40 mJ/cm^2 laser pulse at 532 nm, as measured by a 20 MHz needle hydrophone. b, FFT of the PA waves shown in panels a and c. c, Pressure wave produced by Film B upon pulsed laser excitation at 484 nm of either a 634 μm thick commercial black polystyrene disk (blue line) or of film B (red line), as measured by a 225 MHz contact transducer. d, Dependence of the photoacoustic signal intensity on the thickness of the series of films C1–C5 with matched absorbances at the pulsed laser excitation wavelength of 471.5 nm, as measured by a 100 MHz contact transducer.

laser ON. Films A and B were used in the various experiments, and the laser fluence per pulse was set to 50 mJ/cm^2 (6.25 MW/cm^2).

The TEWL measured on the left and right volar forearms of 12 females and 9 male volunteers aged 18–25 years before the application of PA waves was 14.3 ± 0.6 g cm^{-2} h^{-1} (average ± s.e.m.), in good agreement with the values reported in the literature for the use of the open chamber Tewameter [13]. The average (± s.e.m.) TEWL increase due to simple occlusion with the laser OFF was 5.4 ± 0.9 g/(cm^2 h), while the 2 min exposure to PA waves increased the TEWL by 17 ± 3 g/(cm^2 h). Thus, there is a statistically significant difference (t probability <0.005) between the increase in TEWL due to simple occlusion or to 2 min of PA waves. Fig. 3 presents the TEWL changes and their exponential return to normal values with a half-life of $\tau_{1/2} = 40$ s. Considering that the first TEWL measurement was made 15 s after lifting the material from the skin, to allow for the cleaning of the silicone with absorbing paper, and assuming the same exponential relaxation in the first 15 s, we obtain an initial TEWL increase of 21.5 g/(cm^2 h), and 5.9 g/(cm^2 h) of which are due to the occlusion. This transient increase by 5.9 g/(cm^2 h) comes from near-surface water trapped by occlusion. The remaining increase, 16 g/(cm^2 h), is due to the increased permeability of the skin when subjected to 2 min of PA waves.

Erythema was measured at the site of PA waves exposure before and after the measurement of TEWL, and a significant increase was observed, from 254 ± 8 to 324 ± 15 (t probability <0.0001). This increase is barely perceptive to the view and is resolved in a few minutes. A visual analog scale was employed for rating pain, from 0 (no pain) to 10 (worst pain ever). This scale was employed to score the pain after 2 min of the control (laser OFF) experiments and after 1 min and 2 min of the laser ON experiment. Scores of 0 to 2 were reported with the laser OFF and with 18 volunteers with the laser ON. Two volunteers reported a score of 3 and one a score of 5. The TEWL of this volunteer increased by 40 g/(cm^2 h) and was the second highest registered. The box plot of Fig. 4 clearly shows the volunteer with a score of 5 is also an outlier in the control experiment. Thus, TEWL in healthy volunteers increases by more than factor of 2 after 2 min of exposure to PA waves at 20 Hz, and then the skin recovers its protective function in 2 min, leaving no signs of damage to the skin and causing mostly a gentle warming sensation.

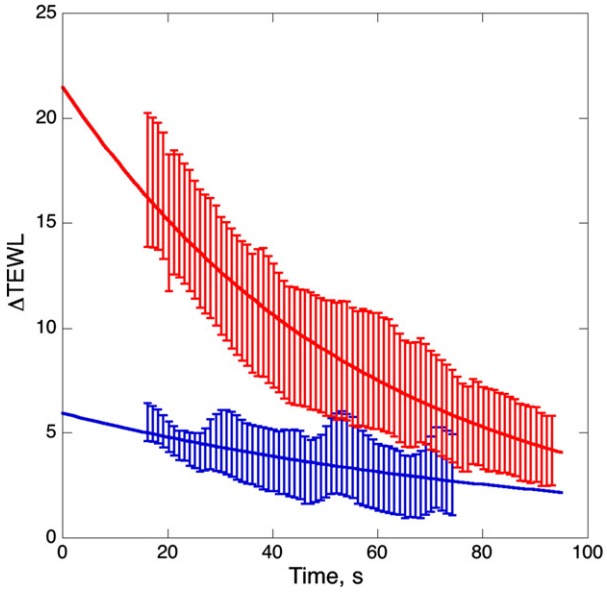

Fig. 3. Changes in transepidermal water loss (average ± s.e.m.) of the right (in red) and left (in blue) ventral forearms of volunteers. The right ventral forearms were exposed for 2 min to PA waves generated by Film A or B while subject to 50 mJ/cm^2 laser pulses at 20 Hz, and the change is the TEWL after the exposure to the PA waves minus the initial TEWL. The TEWL of the left ventral forearms was measured with the same protocol but with the laser off. The silicone used to improve the acoustic coupling was cleaned before the first TEWL measurement reported in each experiment, and this took ca. 15 s.

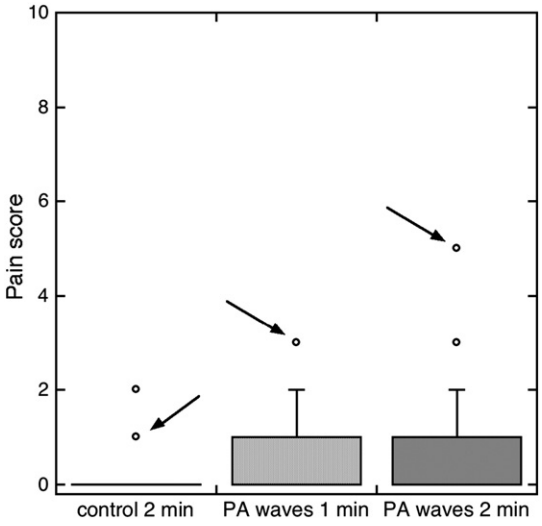

Fig. 4. Box plot of pain reported according to a visual analog scale. No pain = 0, worst pain ever = 10. Each box encloses 50% of the data, and outliers as displayed as individual points. The arrow indicates the same subject that appears as an outlier in the control (laser OFF) and in the experiments with laser ON.

A similar increase by a factor of two in TEWL was reported for 10× sequential tape strippings with D-Squame® tapes [14], and in other similar studies [57], but the increased TEWL remains at the high level for at least two hours after the tape stripping. The effect on TEWL of metal microneedle arrays with needles lengths of 200–400 μm and diameters of 200–300 μm was also recently reported [57]. The increases in TEWL with such microneedles did not reach a factor of two and the largest increases were associated with longer skin recovery times, typically more than two hours [57]. Iontophoresis applied for 3 h at a current density of 250 μA/cm^2, which corresponds to a total delivery current higher than usual for this transdermal delivery technique, showed that the effect of iontophoresis on TEWL is not as pronounced as the effect of simple occlusion [58]. Additionally erythema was observed in all subjects of that study and edema was also occasionally observed.

The rapid increase in TEWL with the application of PA waves followed by an exponential relaxation to baseline values in 2 min seems to be a distinct feature of the broadband PA waves with steep pressure gradients generated in these experiments. It is likely that the gentle warming experienced by some of the volunteers contributes to the increase in TEWL. In fact, Maibach and co-workers [59] quantified the skin temperature dependence of TEWL and using their equations we calculate that a temperature increase from 34 °C to 38 °C may increase the TEWL from 14 to 18 g/(cm^2 h). Ogura and co-workers took advantage of this effect by combining the laser-induced stress waves with skin heating [60], while trying to avoid the use of high peak pressures that are associated with the risk of mechanical damage to the skin. These authors showed that the skin permeability of a photosensitizer used in PDT (Photofrin, which is a mixture of hematoporphyrin derivatives with molecular weights between 1.2 and 4.9 kDa) is enhanced by pressures waves with 520 bar peak pressures and 1 μs pulse widths, generated by laser ablation of black rubber, when the surface temperature of the skin is heated to 48 °C. In our experiments we observed a TEWL increase from 14 to 30 g/(cm^2 h), which means that the expected temperature change (+4 °C, +4 g/(cm^2 h)) is a minor contributor to the observed increase. On the other hand, the PA waves generated in the limits of photoacoustic spectral confinement have the duration of the laser pulse and the rate of pressure increase of a 12 bar PA

wave generated by the absorption of a 6 ns laser pulse by a piezophotonic material is >2 bar/ns. This is remarkably similar to the magnitude of the pressure rise times between 2.5 and 50 bar/ns of the pressure transients reported by Doukas and co-workers [25]. Pressure rise times are related to pressure gradients by the speed of sound and, in tissues, the values above correspond to pressure gradients > 1 bar/μm. Although these methods are based on different approaches to generate pressure transients, they cause similar pressure gradients and should produce the same effects (i.e., the expansion of lacunar domains), which are manifested macroscopically as an increase in the permeabilization of the SC. In summary, the exposure to safe PA waves rapidly increases in the TEWL of healthy volunteers from 14 g/(cm^2 h) to 36 g/(cm^2 h), but the SC recovers its protective function two minutes after the end of such PA waves.

4.3. Drug delivery

The large change in TEWL observed with the application of PA waves generated by piezophotonic materials and the correlation between TEWL and the skin barrier function [14,16–19], suggest that such PA waves can be used to increase the permeability of skin to drugs. The control of skin permeability without causing discomfort or lasting effects is especially interesting for the case of large molecules (>500 Da) and proteins, which have small or negligible flows through the SC. We selected a bacteriochlorin with a molecular weight of 1.1 kDa and GFP (28 kDa) to test the dermal delivery with PA waves because these species cover a range in sizes and structures that is of clinical interest, and also because their fluorescence simplifies the analytical procedures. *In vivo* experiments with minipigs were run 3 years apart, where the first set of experiments investigated mostly safety and the second set were confirmatory experiments with optimized piezophotonic materials. Minipig skin samples collected after the first set of experiments were kept refrigerated and used for various optimization experiments in between *in vivo* experiments. We focus below the *in vivo* studies of drug flow through minipig skin because they are the most adequate to anticipate protocols for eventual clinical studies. Other micrographs illustrating of increased diffusion elicited by PA waves *in vivo* and *post mortem* are presented as Supplementary Data.

Fig. 5 presents representative confocal microscopy images of *in vivo* experiments with minipigs using a topical formulation of the bacteriochlorin. In the passive delivery experiment, the formulation was placed in contact with the skin and occluded for 2 h before the animal was sacrificed. In the active delivery experiment, the same formulation was placed 20 min before the sacrifice of the animal, subject to PA waves generated with film E for 25 s with a 20 Hz repetition rate, and occluded. Skin biopsies were collected just before the death of the animal. After the treatment of the skin biopsies, confocal microscopy revealed that the depth of diffusion increased from 15 μm for passive diffusion in 2 h (Fig. 5A) to 35 μm in 30 min with the application of PA waves (Fig. 5B). This is consistent with the role of stress waves with steep pressure gradients in disturbing temporarily the SC [24], with the measurements of TEWL and with the ability of the molecules to diffuse more easily in the epidermis. It must be emphasized that the TEWL measurements in volunteers did not employ any permeation enhancer, whereas the formulations used for passive and active delivery included oleic acid or Azone in their compositions. Penetration enhancers are known to extend the transient increase of skin permeability induced of stress waves [61].

Confocal microscopy is appropriate to assess the depth of permeation of fluorescent drugs, but the quantification of the flow of a drug through a given surface area of skin requires other analytical techniques. The flow was investigated extracting the bacteriochlorin from minipig skin biopsies collected after different contact times of the topical formulation with the skin. The amount of bacteriochlorin extracted was then quantified by fluorescence using a calibration curve. The calibration curve in the Supplementary Data illustrates the sensitivity and accuracy of this technique in the nanomolar concentration range. The distinctive fluorescence of tetraphenylbacteriochlorins near 750 nm avoids contaminations with endogenous fluorophores [62]. Passive delivery employed contact times of the formulation with the minipig skin, under occlusion, of 30 min, 1 h, 2 h and 3 h. The contact times for active delivery with oleic acid as permeation enhancer were 15 min, 30 min and 1 h. In all the experiments, the contact times were programmed to finish at the same time, and at that time the minipigs were sacrificed.

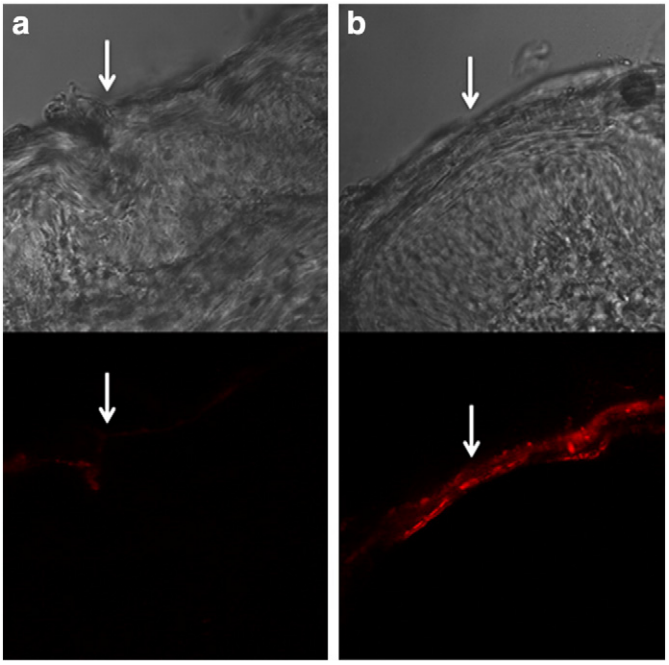

Fig. 5. Representative microscopy images of minipig skin biopsies after *in vivo* transdermal delivery of a bacteriochlorin. a, Confocal microcopy of a 1.1 kDa bacteriochlorin after 2 h of passive diffusion (λ_{ex} = 514 nm, λ_{em} ≥ 650 nm, laser power at 5%, amplification 40×). b, Confocal microscopy of the same bacteriochlorin (under the same conditions) 30 min after the photoacoustic delivery with Film E and 50 mJ/cm^2 laser pulses at 20 Hz for 25 s.

The mass of bacteriochlorin extracted in the passive delivery experiments with oleic acid increases with time, from 0.031 ± 0.006 μg at 30 min to 0.089 ± 0.016 μg at 3 h. When PA waves were applied, the average mass extracted between 15 and 60 min of contact of the same formulation with the skin was 0.082 ± 0.016 μg. An alternative formulation using Azone as permeation enhancer was also tested. The average mass extracted after 1 h of passive delivery with this formulation was 0.025 ± 0.009 μg and remained at this level after 3 h, whereas with the application of the PA waves the average mass extracted between 5 and 16 min of skin contact was 0.086 ± 0.020 μg. The passive permeation with oleic acid is better than with Azone, but the active permeation is not very sensitive to the permeation enhancer. The detailed statistics are presented in the Supplementary Data.

Fig. 6 compares the fluxes obtained with PA waves and with passive delivery, both employing oleic acid as permeation enhancer. It is clear the effect of the PA waves generated with Film E and 8 ns laser pulses (fluences of 25 or 50 mJ/cm^2) at 20 Hz for 25 s was most pronounced in the first 15 min after the application of the PA waves and that this translated in an active flow of 2.6 ± 0.6 μg/(cm^2 h). After 30 min the flux measured for the active permeation, 1.3 ± 0.2 μg/(cm^2 h), is still significantly ($p<0.05$) higher than that of the passive permeation, 0.49 ± 0.09 μg/(cm^2 h), but after one hour the difference is no longer significant. This is entirely consistent with the TEWL, and reflects the recovery of the barrier function of the SC after the perturbation with

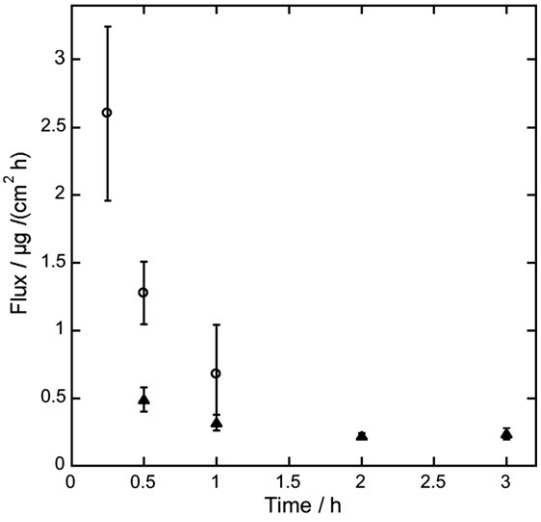

Fig. 6. Fluxes obtained with PA waves and with passive delivery. The same formulation with bacteriochlorin and oleic acid was used in both experiments. The PA waves were generated with Film E and 8 ns laser pulses (fluences of 25 or 50 mJ/cm^2) at 20 Hz for 25 s.

PA waves. This recovery is expected to take place in a few minutes and the active flux must converge to the passive flux as the skin fully recovers. Time averaging of the fluxes attenuates the differences for longer contact times between the formulation and the skin. The active flux measured for the formulation with Azone corroborates these findings, as it decreases from 5.9 ± 1.5 μg/(cm^2 h) in the first 10 min to 1.2 ± 0.2 μg/(cm^2 h) in the first 30 min (see Supplementary Data). In the case of the formulation with oleic acid, the active flux of the bacteriochlorin 15 min after the application of PA waves is 5.3 times higher than the highest passive flux with this formulation.

Following the successful administration of a large molecule with PA waves, the transdermal delivery of GFP was attempted with the same gel base formulation. GPF was incorporated to reach 0.1% the gel base, which contained 4% of Azone. The formulation was placed in contact with the skin of a minipig for 4 h. However, the passive dermal delivery of GFP in this topical formulation failed to lead to measurable GFP fluorescence in skin biopsies. On the other hand, when the same formulation was placed in contact with the skin of minipigs and it was subject to 12 PA waves with Film F or 6 PA waves with Film G, extensive GFP distribution in the epidermis was found after 20 min of contact of the formulation with the skin, as shown in Fig. 7. GFP fluorescence and confocal microscopies refer *in vivo* and *postmortem* topical experiments, respectively. The SC remained intact after all the experiments.

The micrographs of Fig. 7 suggest that GFP diffused by $h \approx 50$ μm in $t = 20$ min. Under these conditions its diffusion coefficient is $D = h^2/(2\ t) \approx 10^{-8}$ cm^2/s, which is one order of magnitude below the diffusion coefficient of yellow fluorescent protein in cells [63]. The diffusion coefficient of proteins is related to the molecular weight M, temperature T and viscosity η of the medium [64]

$$D = 8.34\text{x}10^{-8}\ T/\left(\eta M^{1/3}\right) \tag{5}$$

We obtain $\eta \approx 20$ cp at $T = 37$ °C, which is close to the viscosity of oleic acid at the same temperature. These are physically realistic values for the diffusion coefficient and medium viscosity.

Seminal work on the permeabilization of skin to large drugs with a single high pressure wave was published by Doukas and co-workers [25], which included insulin in their pallet of drugs [65]. These authors emphasized that the ablation of polystyrene targets by laser pulses with fluences ca. 5 J/cm^2 can generate pressure waves with amplitudes between 300 and 1000 bar, that are much more effective

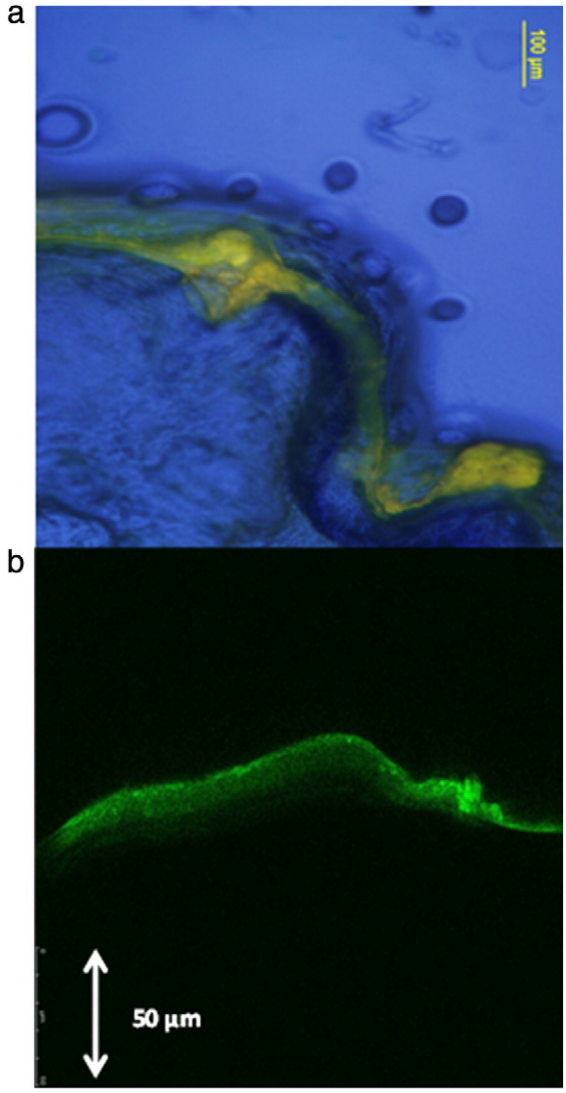

Fig. 7. Representative microscopy images of minipig skin biopsies after transdermal delivery of GFP. a, Fluorescence microscopy of GFP (excitation filter 470–495 nm, emission filter 510–550 nm) in biopsies collected 20 min after photoacoustic delivery with Film F and 12 laser pulses at a fluence of 10 mJ/cm^2. d, Confocal microscopy of GFP in biopsies ($\lambda_{ex} = 488$ nm, $\lambda_{em} \geq 495$ nm, laser power at 50%) collected 20 min after photoacoustic delivery with Film G and 6 laser pulses at a fluence of 50 mJ/cm^2.

in permeabilizing the SC than the pressure waves with amplitudes of 1 to 5 bar usually generated in conventional ultrasound techniques. It was further observed that the onset of SC permeabilization occurred at 350 bar [25]. Ogura and co-workers used stress waves with 520 bar peak pressures and 1 μs pulse widths for the same purpose [60]. Our work shows the increase in the permeability of the SC to water, to a 1.1 kDa molecule and to a 28 kDa protein with PA waves having amplitudes ca. 10 bar generated with laser fluences lower than 50 mJ/cm^2. These studies have in common the use of pressure gradients larger than 1 bar/μm. The PA waves generated with piezophotonic materials attain such large pressure gradients with peak pressures below 20 bar and Mechanical Indices below the cavitation threshold because of they have significant ultrasonic frequencies above 100 MHz.

5. Conclusions

Light-to-pressure transduction was improved using thin materials with a large Grüneisen coefficients and incorporating in such materials a dye that gives the following properties to the (piezophotonic) material: i) $\mu_a > 100$ cm^{-1} at the incident laser light, ii) ultrafast

radiationless decays to the ground state. When piezophotonic materials absorb short laser pulses (<10 ns) with modest laser fluences (<50 mJ/cm^2), they generate PA waves with moderate peak pressures (<50 bar) but very high rise times (>1 bar/ns) that transiently permeabilize the stratum corneum to large molecules and proteins. PA waves with these properties increased the TEWL of human skin in a painless and reversible manner. Such PA waves also increased significantly the initial fluxes of a 1.1 kDa molecule and a 28 kDa protein through the stratum corneum of minipigs. The transient impairment of the skin barrier function was observed for a wide range of skin conditions (defrosted skin to *in vivo*), molecular sizes and polarities of skin permeants (water to GFP), and laser pulses (single-shot to 20 Hz, 25 to 50 mJ/cm^2).

Acknowledgments

We thank RedEmprendia (AVCRI prize) for the financial support and Luzitin SA (Portugal) for the sample of the bacteriochlorin. GFFS thanks FCT for the PhD grant BD/45555/2008. We specially thank Dr. Ramiro Mascarenhas, veterinary surgeon at INRB, for the invaluable assistance with the minipig experiments, Prof. M.M. Pereira for the porphyrin derivatives, Prof. J. M. M. Martinho (IST, Portugal) and Dr. L. Cortes (CNC-Coimbra, Portugal) for assistance with confocal microscopy, and Patricia Jesus for the preparation of TiO_2 films.

Appendix A. Supplementary data

Supplementary data to this article can be found online at http://dx.doi.org/10.1016/j.jconrel.2013.02.005.

References

[1] M.R. Prausnitz, R. Langer, Transdermal drug delivery, Nat. Biotechnol. 26 (2008) 1261–1268.
[2] B.M. Magnusson, Y.G. Anissimov, S.E. Cross, M.S. Roberts, Molecular size as the main determinant of solute maximum flux across the skin, J. Investig. Dermatol. 122 (2004) 993–999.
[3] C. Lipinski, F. Lombardo, B. Dominy, P. Feeney, Experimental and computational approaches to estimate solubility and permeability in drug discovery and development settings, Adv. Drug Deliv. Rev. 46 (2001) 3–26.
[4] P. Karande, A. Jain, K. Ergun, V. Kispersky, S. Mitragotri, Design principles of chemical penetration enhancers for transdermal drug delivery, Proc. Natl. Acad. Sci. U. S. A. 102 (2005) 4688–4693.
[5] M.B. Brown, G.P. Martin, S.A. Jones, F.K. Akomeah, Dermal and transdermal drug delivery systems: current and future prospects, Drug Deliv. 13 (2006) 175–187.
[6] G. Cevc, U. Vierl, Nanotechnology and the transdermal route. A state of the art review and critical appraisal, J. Control. Release 141 (2010) 277–299.
[7] J.J. Escobar-Chávez, D. Bonilla-Martínez, M.A. Villegas-González, E. Molina-Trinidad, N. Casa-Alancater, A.L. Revilla-Vázquez, Microneedles: a valuable physical enhancer to increase transdermal drug delivery, J. Clin. Pharmacol. 51 (2011) 964–977.
[8] J.W. Lee, P. Gadiraju, J.-H. Park, M.G. Allen, M.P. Prausnitz, Microsecond thermal ablation of skin for transdermal drug delivery, J. Control. Release 154 (2011) 58–68.
[9] B.E. Polat, D. Hart, R. Langer, D. Blankschtein, Ultrasound-mediated transdermal drug delivery: mechanisms, scope, and emerging trends, J. Control. Release 152 (2011) 330–348.
[10] I. Iwai, H. Han, L. den Hollander, S. Svensson, L.-G. Öfverstedt, J. Anwar, J. Brewer, M. Bloksgaard, A. Laloeuf, D. Nosek, S. Masich, L.A. Bagatolli, U. Skoglund, L. Norlén, The human skin is organized as stacked bilayers of fully extended ceramides with cholesterol molecules associated with the ceramide sphingoid moiety, J. Investig. Dermatol. 132 (2012) 2215–2225.
[11] J. Pinnagoda, R.A. Tupker, T. Agner, J. Serup, Guidelines for transepidermal water loss (TEWL) measurement, Contact Dermat. 22 (1990) 164–178.
[12] G. Yosipovitch, G.L. Xiong, E. Haus, L. Sackett-Lundeen, I. Ashkenazi, H. Maibach, Time-dependent variations of the skin barrier function in humans: transepidermal water loss, stratum corneum hydration, skin surface pH, and skin temperature, J. Investig. Dermatol. 110 (1998) 20–23.
[13] K. De Paepe, E. Houben, R. Adam, F. Wiesemann, V. Rogiers, Validation of the VapoMeter, a closed unventilated chamber system to assess transepidermal water loss vs. the open chamber Tewameters, Skin Res. Technol. 11 (2005) 61–69.
[14] J.W. Fluhr, K.R. Feingold, P.M. Elias, Transepidermal water loss reflects permeability barrier status: validation in human and rodent in vivo and ex vivo models, Exp. Dermatol. 15 (2006) 483–492.
[15] P. Kleesz, R. Darlenski, J.W. Fluhr, Full-body skin mapping for six biophysical parameters: baseline values at 16 anatomical sites in 125 human subjects, Skin Pharmacol. Physiol. 25 (2012) 25–33.
[16] J. Levin, H. Maibach, The correlation between transepidermal water loss and percutaneous absorption: an overview, J. Control. Release 103 (2005) 291–299.
[17] K. Shimada, T. Yoshihara, M. Yamamoto, K. Konno, Y. Momoi, K. Nishifuji, T. Iwasaki, Transepidermal Water Loss (TEWL) reflects skin barrier function of dog, J. Vet. Med. Sci. 70 (2008) 841–843.
[18] M. Machado, T.M. Salgado, J. Hadgraft, M.E. Lane, The relationship between transepidermal water loss and skin permeability, Int. J. Pharm. 384 (2010) 73–77.
[19] L. Rubio, C. Alonso, O. López, G. Rodríguez, L. Coderch, J. Notario, A. de la Maza, J.L. Parra, Barrier function of intact and impaired skin: percutaneous penetration of caffeine and salicylic acid, Int. J. Dermatol. 50 (2011) 881–889.
[20] D. Bommannan, G.K. Menon, H. Okuyama, P.M. Elias, R.H. Guy, Sonophoresis. II. Examination of the mechanism(s) of ultrasound-enhanced transdermal drug delivery, Pharm. Res. 9 (1992) 1043–1047.
[21] S. Paliwal, G.K. Menon, S. Mitragotri, Low-frequency sonophoresis: ultrastructural basis for stratum corneum permeability assessed using quantum dots, J. Investig. Dermatol. 126 (2006) 1095–1101.
[22] S.E. Lee, K.J. Choi, G.K. Menon, H.J. Kim, E.H. Choi, S.K. Ahn, S.H. Lee, Penetration pathways induced by low-frequency sonophoresis with physical and chemical enhancers: iron oxide nanoparticles versus lanthanum nitrates, J. Investig. Dermatol. 130 (2010) 1063–1072.
[23] G.K. Menon, P.M. Elias, in: U.R. Hengge, B. Volc-Platzer (Eds.), The Skin and Gene Therapy, Spinger-Verlag, Berlin, 2001, pp. 3–26.
[24] G.K. Menon, N. Kollias, A.G. Doukas, Ultrastructural evidence of stratum corneum permeabilization induced by photomechanical waves, J. Investig. Dermatol. 121 (2003) 104–109.
[25] A.G. Doukas, N. Kollias, Transdermal delivery with a pressure wave, Adv. Drug Deliv. Rev. 56 (2004) 559–579.
[26] H.K. Park, D. Kim, C.P. Grigoropoulos, A.C. Tam, Pressure generation and measurement in the rapid vaporization of water on a pulsed-laser-heated surface, J. Appl. Phys. 80 (1996) 4072–4081.
[27] E. Biagi, F. Margheri, D. Menichelli, Efficient laser-ultrasound generation by using heavily absorbing films as targets, IEEE Trans. Ultrason. Ferroelectr. Freq. Control 48 (2001) 1669–1680.
[28] G.V. Ostrovskaya, Optical-to-acoustic energy conversion efficiency upon interaction of pulsed laser radiation with a liquid: II. Conversion efficiency measurement by holographic interferometry upon acoustooptic interaction, Tech. Phys. 47 (2002) 1547–1553.
[29] M.W. Sigrist, Laser generation of acoustic waves in liquids and gases, J. Appl. Phys. 60 (1986) R83–R121.
[30] J.-P. Simonin, On the mechanisms of in vitro and in vivo phonophoresis, J. Control. Release 33 (1995) 125–141.
[31] W.H. Childs, Thermomechanical properties of selected space-related materials, The Aerospace Corporation, Los Angeles, TR-2002(8565)-7, 30 Sept 2001 2002.
[32] Z. Pu, in: J.E. Mark (Ed.), Polymer Data Handbook, Oxford University Press, Oxford, 1999, pp. 829–836.
[33] H. Fukumura, N. Mibuka, S. Eura, H. Masuhara, N. Nishi, Mass spectrometric studies on laser ablation of polystyrene sensitized with anthracene, J. Phys. Chem. 97 (1993) 13761–13766.
[34] L.V. Zhigilei, B.J. Garrison, Microscopic mechanisms of laser ablation of organic solids in the thermal and stress confinement irradiation regimes, J. Appl. Phys. 88 (3) (2000) 1281–1298.
[35] A.A. Karabutov, E.V. Savateeva, N.B. Podymova, A.A. Oraevsky, Backward mode detection of laser-induced wide-band ultrasonic transients with optoacoustic transducer, J. Appl. Phys. 87 (2000) 2003–2014.
[36] M. Pineiro, A.L. Carvalho, M.M. Pereira, A.M.d.A.R. Gonsalves, L.G. Arnaut, S.J. Formosinho, Photoacoustic measurements of porphyrin triplet state quantum yields and singlet oxygen efficiencies, Chem. Eur. J. 4 (1998) 2299.
[37] F.A. Schaberle, R.M.D. Nunes, M. Barroso, C. Serpa, L.G. Arnaut, Analytical solution for time-resolved photoacoustic calorimetry data. A survey of mechanisms common in photochemistry, Photochem. Photobiol. Sci. 9 (2010) 812–822.
[38] E.F. Carome, N.A. Clark, C.E. Moeller, Generation of acoustic signals in liquids by Ruby laser-induced thermal stress transients, Appl. Phys. Lett. 4 (1964) 95–97.
[39] R.J. von Gutfeld, R.L. Melcher, 20 MHz acoustic waves from pulsed thermoelastic expansions of constrained surfaces, Appl. Phys. Lett. 30 (1977) 257–259.
[40] L.G. Arnaut, R.A. Caldwell, J.E. Elbert, L.A. Melton, Recent advances in photoacoustic calorimetry: theoretical basis and improvements in experimental design, Rev. Sci. Instrum. 63 (1992) 5381–5389.
[41] Y. Guo, H.W. Baac, S.-L. Chen, T.B. Norris, L.J. Guo, Broad-band, high-efficiency optoacoustic generation using a novel photonic crystal-metallic structure, Proc. SPIE 78992 (2011) 78992C.
[42] C. Serpa, J. Schabauer, A.P. Piedade, C.J.P. Monteiro, M.M. Pereira, P. Douglas, H.D. Burrows, L.G. Arnaut, Photoacoustic measurement of electron injection efficiencies and energies from excited sensitizer dyes into nanocrystalline TiO_2 films, J. Am. Chem. Soc. 130 (2008) 8876–8877.
[43] J.M. Dabrowski, L.G. Arnaut, M.M. Pereira, K. Urbanska, S. Simões, G. Stochel, L. Cortes, Combined effects of singlet oxygen and hydroxyl radical in photodynamic therapy with photostable bacteriochlorins: evidence from intracellular fluorescence and increased photodynamic efficacy in vitro, Free Radic. Biol. Med. 55 (2012) 1188–1200.
[44] J.M. Dabrowski, L.G. Arnaut, M.M. Pereira, K. Urbanska, G. Stochel, Improved biodistribution, pharmacokinetics and photodynamic efficacy using a new photostable sulfonamide bacteriochlorin, Med. Chem. Commun. 3 (2012) 502–505.
[45] M. Dubois, P.W. Lorraine, B. Venchiarutti, A.S. Bauco, R.J. Filkins, T.E. Drake, K.R. Yawn, in: D. Thompson, D. Chimenti (Eds.), Review of Progress in Quantitative Nondestructive Evaluation, AIP Conf. Proc., vol. CP509, 2000, p. 287.

[46] V.V. Kozhushko, P. Hess, Laser-induced ultrasound for nondestructive testing and evaluation, J. Appl. Phys. 103 (2008) 124902.
[47] R.E. Apfel, C.K. Holland, Gauging the likelihood of cavitation from short-pulse, low-duty cycle diagnostic ultrasound, Ultrasound Med. Biol. 17 (1991) 179–185.
[48] J. Wu, W.L. Nyborg, Ultrasound, cavitation bubbles and their interaction with cells, Adv. Drug Deliv. Rev. 60 (2008) 1103–1116.
[49] R.S. Meltzer, Food and Drug Administration ultrasound device regulation: the output display standard, the "mechanical index", and ultrasound safety, J. Am. Soc. Echocardiogr. 9 (1996) 216–220.
[50] NCRP, Exposure criteria for medical diagnostic ultrasound. II. Criteria based on all known mechanisms, National Council on Radiation Protection and Measurements, Bethesda MD, 2002.
[51] S. Mitragotri, D.A. Edwards, D. Blankshtein, R. Langer, A mechanistic study of ultrasonically-enhanced transdermal drug delivery, J. Pharm. Sci. 84 (1995) 697–706.
[52] B. Krasovitski, V. Frenkel, S. Shoham, E. Kimmel, Intramembrane cavitation as a unifying mechanism for ultrasound-induced bioeffects, Proc. Natl. Acad. Sci. U. S. A. 108 (2011) 3258–3263.
[53] A. Tezel, S. Mitragotri, Interactions of inertial cavitation bubbles with stratum corneum lipid bilayers during low-frequency sonophoresis, Biophys. J. 85 (2003) 3502–3512.
[54] K. Hynynen, The threshold for thermally significant cavitation in dog's thigh muscle in vivo, Ultrasound Med. Biol. 17 (1991) 157–169.
[55] S. Lee, D.J. McAuliffe, T.J. Flotte, N. Kollias, A.G. Doukas, Photomechanical transcutaneous delivery of macromolecules, J. Investig. Dermatol. 111 (1998) 925–929.
[56] O.A. Sapozhnikov, V.A. Khokhlova, M.R. Bailey, J.C. Williams Jr., J.A. McAteer, R.O. Cleveland, L.A. Crum, Effect of overpressure and pulse repetition frequency on cavitation in shock wave lithotripsy, J. Acoust. Soc. Am. (2002) 1183–1195.
[57] S.M. Ball, J. Caussin, S. Pavel, J.A. Bouwstra, In vivo assessment of safety of microneedle arrays in human skin, Eur. J. Pharm. Sci. 35 (2008) 193–202.
[58] G.L. Li, T.J. Van Steeg, H. Putter, J. Van der Spek, S. Pavel, M. Danhof, J.A. Bouwstra, Cutaneous side-effects of transdermal iontophoresis with and without surfactant pretreatment: a single-blinded, randomized controlled trial, Br. J. Dermatol. 153 (2005) 404–412.
[59] C.G.T. Mathias, M.D. Donald, M.D. Wilson, H.I. Maibach, Transepidermal water loss as a function of skin temperature, J. Investig. Dermatol. 77 (1981) 219–220.
[60] M. Ogura, S. Sato, M. Kuroki, H. Wakisaka, S. Kawauchi, M. Ishihara, M. Kikuchi, M. Yoshioka, H. Ashida, M. Obara, Transdermal delivery of photosensitizer by the laser-induced stress wave in combination with skin heating, Jpn. J. Appl. Phys., Part 2 - Lett. 41 (7A) (2002) L814–L816.
[61] S. Lee, D.J. McAuliffe, N. Kollias, T.J. Flotte, A.G. Doukas, Permeabilization and recovery of the stratum corneum in vivo: the synergy of photomechanical waves and sodium lauryl sulfate, Lasers Surg. Med. 29 (2001) 145–150.
[62] J.M. Dabrowski, K. Urbanska, L.G. Arnaut, M.M. Pereira, A.R. Abreu, S. Simões, G. Stochel, Biodistribution and photodynamic efficacy of a water-soluble, stable halogenated bacteriochlorin against melanoma, ChemMedChem 6 (2011) 465–475.
[63] T. Kühn, T.O. Ihalainen, J. Hyväluoma, N. Dross, S.F. Willman, J. Langowski, M. Vihinen-Ranta, J. Timonen, Protein diffusion in mammalian cell cytoplasm, PLoS One 6 (2011) e22962.
[64] M.E. Young, P.A. Carroad, R.L. Bell, Estimation of diffusion coefficients of proteins, Biotechnol. Bioeng. 22 (1980) 947–955.
[65] S. Lee, D.J. McAuliffe, S.E. Mulholland, A.G. Doukas, Photomechanical transdermal delivery of insulin in vivo, Lasers Surg. Med. 28 (2001) 282–285.